



HAL
open science

Polar surface of ferroelectric nanodomains in GeTe thin films

B. Croes, F. Cheynis, P. Müller, S. Curiotto, F. Leroy

► **To cite this version:**

B. Croes, F. Cheynis, P. Müller, S. Curiotto, F. Leroy. Polar surface of ferroelectric nanodomains in GeTe thin films. *Physical Review Materials*, 2022, 6 (6), pp.064407. 10.1103/PhysRevMaterials.6.064407 . hal-03778329

HAL Id: hal-03778329

<https://hal.science/hal-03778329>

Submitted on 15 Sep 2022

HAL is a multi-disciplinary open access archive for the deposit and dissemination of scientific research documents, whether they are published or not. The documents may come from teaching and research institutions in France or abroad, or from public or private research centers.

L'archive ouverte pluridisciplinaire **HAL**, est destinée au dépôt et à la diffusion de documents scientifiques de niveau recherche, publiés ou non, émanant des établissements d'enseignement et de recherche français ou étrangers, des laboratoires publics ou privés.

Polar surface of ferroelectric nanodomains in GeTe thin films

B. Croes,¹ F. Cheynis,¹ P. Müller,¹ S. Curiotto,¹ and F. Leroy¹

¹*Aix Marseille Univ, CNRS, CINAM, AMU-TECH, Marseille, France*

(Dated: June 1, 2022)

Ferroelectrics have polar surfaces that can undergo large structural and stoichiometric modifications to be neutral. These changes can have major implications on the surface stability and physico-chemical properties. We have studied the growth and structure of ferroelectric GeTe thin films on Si(111) by a combination of scanning tunneling microscopy, low energy electron microscopy and low energy electron diffraction. We show that the GeTe growth occurs with a single epitaxy and proceeds via a step-flow mode hindered by the advance of electrically neutral step edges exhibiting triangular notches. We demonstrate the presence of ferroelectric nanodomains with in-plane component of polarization and a complex restructuring of their polar surface. 2×2 surface reconstruction, missing row reconstruction and extended 2D modulations of the surface structure are demonstrated on these nanodomains. We show that these structures stabilize the surface termination of the low-symmetry polar nanodomains.

Ferroelectric thin films are the object of intense fundamental research stimulated by their applications as functional materials based on the existence of different polar variants. The main factors that govern the spatial organization of ferroelectric domains are the elastic interactions that arise from the electromechanical coupling between domains and the electrostatic interactions due to local exceeding charges. The ability to synthesize ferroelectric thin films of high crystalline quality based on layer-by-layer growth techniques and to engineer the strain field *via* the substrate choice have made possible to exploit these interactions and discover novel phenomena. It has been demonstrated that flux-closure polar domains [1–3], vortices [4 and 5] and even skyrmions [6] could be obtained in ferroelectric materials. This has led to a renewed interest [7–9] for prior studies on incommensurate phases in ferroelectrics with the observation of one-dimensional stripe domain patterns or even more complex 2D modulations as observed in the structural phase transitions of α - β quartz [10]. The experimental studies of the structure of ferroelectric materials are mainly based on the atomic scale characterization of domain boundaries and interfaces by STEM [11] and X-ray diffraction [12 and 13]. The surface structure of ferroelectrics has been much less explored. However the surface is also a place where charge screening and stress relaxation occur on atomic scale distances. In particular it has been recognized since a long time that a polar surface, *i.e.* a surface cut perpendicular to a direction along which the unit cell carries a net electric dipole moment, requires major rearrangements to solve the problem of the divergence of the electrostatic potential [14]. Several charge compensation mechanisms have been proposed to stabilize polar surfaces: purely electronic effects, modifications of the surface structure/stoichiometry or adsorption/segregation of charged species [15]. Moreover since the polarization and strain gradient can couple together at the surface through the flexoelectric effect, we can expect that surface modulations or ripples can be favored [16 and 17]. Therefore, surface studies may provide new insight into the fundamental properties of ferroelectric

materials and this point is all the more crucial that mass transport processes during thin film growth occur at surfaces and may be strongly influenced by these surface modifications [18 and 19].

Among ferroelectrics, a new class of materials with high potentialities for spintronic applications has been introduced and known as ferroelectric Rashba semiconductors [20]. Major results have been obtained on α -GeTe thin films. It has been demonstrated the reversal of the ferroelectric polarization under an electric field [21] and a consistent change of the spin chirality of the band structure [22 and 23]. The α -GeTe ferroelectric phase has a rhombohedral structure (space group R3m) and bulk Curie temperature of $T_c \sim 650 - 700$ K. The spontaneous polarization of α -GeTe is along the pseudocubic $\langle 111 \rangle$ leading to the formation of 4 ferroelastic variants and three possible polarization switching between domains at 71° , 109° or 180° . As reported by Wang et al. [24] α -GeTe thin films can be grown on Si(111) by molecular beam epitaxy with a quasi-single crystalline order using a pre-deposition of 1 ML of Sb onto the substrate. Croes et al. [25] have shown that such α -GeTe thin film is an ideal platform to study and control ferroelectric nanodomains as they are no more limited by grain boundaries. The α -GeTe thin films are made of main domains with a ferroelectric polarization perpendicular to the surface, *i.e.* in the [111] direction and called *c*-domains, and ferroelectric nanodomains with a majority of 71° -type domain walls and called hereafter *a*-domains. In this article we address the surface morphology and structure of α -GeTe thin films grown on Si(111). From low energy electron microscopy (LEEM) and scanning tunneling microscopy (STM) studies we show that α -GeTe thin films grow *via* a step-flow mode of Ge-Te bilayers. The growth velocity is limited by the advance of step edges exhibiting triangular notches. Atomic details of the polar surface of α -GeTe indicate that the surface of the GeTe *c*-domains is unreconstructed and Te-terminated. On the contrary the polar surface of the ferroelectric *a*-domains exhibits complex restructuring of the surface: a 2×2 surface reconstruction that is Ge-terminated, a missing row recon-

87 struction and a large scale 2D structure ($\sim 4 \times 5 \text{ nm}^2$) that
 88 stabilizes the surface. We show that these atomic rear-
 89 rangements involve large Te mass transfers.

90 I. EXPERIMENTAL SECTION

91 Si(111) wafers (Siltronix; $550 \mu\text{m}$ -thick; $\rho=1\text{-}10 \Omega\text{cm}$)
 92 are first cleaned by acetone and ethanol rinsing before in-
 93 troduction in ultra-high vacuum (UHV, 10^{-8} Pa). Then
 94 the substrates are degassed at 1000 K during 12 h fol-
 95 lowed by repeated high temperature annealing (1500 K)
 96 during a few minutes in order to obtain a clean 7×7
 97 surface reconstruction. A deposition of 1 ML of Sb is
 98 performed on the Si(111) surface, forming the so-called
 99 Si(111)- $\sqrt{3} \times \sqrt{3}$ -Sb reconstruction that greatly improves
 100 the crystalline quality of the GeTe layer. The GeTe
 101 thin films are grown by co-deposition of Ge ($1175 \text{ }^\circ\text{C}$)
 102 and Te ($310 \text{ }^\circ\text{C}$) in UHV at $275 \text{ }^\circ\text{C}$ and pre-characterized
 103 by *in situ* RHEED. All the deposition sources are effu-
 104 sion cells from MBE-Komponenten GmbH. After growth,
 105 the GeTe layers are transferred under UHV conditions
 106 thanks to a homemade transfer suitcase and character-
 107 ized by low energy electron microscopy (LEEM), low en-
 108 ergy electron diffraction (LEED) using a LEEM III mi-
 109 croscope (Elmitec GmbH) and scanning tunneling mi-
 110 croscope (STM) by a VT-STM (Omicron GmbH). LEEM
 111 images were obtained in bright field mode at an incident
 112 electron energy of 26 eV where a local maximum of re-
 113 flectivity occurs. At this energy the reflected electrons
 114 by the GeTe *c*-domains and by the tilted ferroelectric
 115 *a*-nanodomains are clearly separated in the focal plane.
 116 This allows to use the smallest contrast aperture ($\varnothing=10$
 117 μm) to select only the reflected beam from the *c*-domains
 118 (see Figure 1(a)). STM images were obtained at room
 119 temperature in constant current mode with typical imag-
 120 ing conditions ($U=-1 \text{ V}$, $I=20 \text{ pA}$, W tip). *In situ* STM
 121 characterization of the *a*-nanodomains evolution under
 122 thermal annealing were performed at constant tempera-
 123 ture in the range $200\text{-}250 \text{ }^\circ\text{C}$. The internal structure of
 124 GeTe thin films has been studied by X-ray diffraction
 125 at BM32 beamline (ESRF) and High Resolution TEM.
 126 X-ray diffraction data have been measured at 18 keV
 127 [0.06888 nm] with a beam size of $200 \times 300 \mu\text{m}^2$ and
 128 collected onto a 2D detector. The data analysis consists
 129 of a field correction (of the possible non-uniform response
 130 of the various pixels of the detector) and then a conver-
 131 sion of the measured data from the detector coordinates
 132 (pixel index) to diffraction angles and thus to reciprocal
 133 space coordinates [26]. The 3D reciprocal space maps
 134 have been visualized using the ParaView software. TEM
 135 investigations were performed along $[\bar{1}\bar{1}0]$ zone axis at
 136 an accelerating voltage of 300 kV on a JEOL JEM-3010
 137 instrument with a spatial resolution of 0.17 nm .

II. RESULTS AND DISCUSSION

A. Growth and structure of *a*-nanodomains

140 The surface morphology of a 470 nm -thick GeTe thin
 141 film grown on Si(111) is observed by LEEM (figure 1(a)).
 142 It shows extended flat areas separated by depressions and
 143 needle shape *a*-nanodomains extended in the $\langle 1\bar{1}0 \rangle$ direc-
 144 tion in cubic coordinates of the Si substrate. The LEED
 145 pattern of the surface shows that the threefold symme-
 146 try (figure 1(b)-i) can be associated with the growth of
 147 (111) planes of GeTe on Si(111). Using the diffracted
 148 spots for LEEM imaging (dark-field imaging mode) we
 149 see that only a small fraction of twinned grains are de-
 150 tected at the surface of the thin film (ACB stacking in-
 151 stead of ABC, see figure 1(b)-ii and -iii). These results
 152 indicate a majority epitaxy of $\alpha\text{-GeTe}$ (111) \parallel Si(111) and
 153 $[\bar{1}\bar{1}0]\parallel$ Si $[\bar{1}\bar{1}0]$ [24]. We can also detect by LEEM typical
 154 regular rows of defects on the terraces displaying a char-
 155 acteristic bright/dark contrast (see dashed rectangles in
 156 figure 1(a)). These structures have a period L in the
 157 range $50\text{-}100 \text{ nm}$ and extend over $0.2 - 1 \mu\text{m}$ distance.
 158 They are characteristics of dislocations at small-angle
 159 grain boundaries that are associated with an azimuthal
 160 misorientation $\Delta\theta$ between two neighboring grains [27].
 161 From the periodicity of the defects we can estimate the lo-
 162 cal misorientation of the lattices as $\Delta\theta \sim \frac{a}{L} \sim 0.2^\circ - 0.4^\circ$
 163 that is within the expected angular range deduced from
 164 X-ray measurements of the in-plane mosaicity [24]. The
 165 surface is also covered with elongated *a*-nanodomains.
 166 These nanodomains appear as dark needles in bright
 167 field LEEM imaging mode since the reflected beams from
 168 these *a*-domains are angularly distant. Indeed the LEED
 169 pattern shows that the main reflected beam by the sur-
 170 face is surrounded by three additional secondary reflected
 171 beams (figure 1(e)). Since the angular shift of these
 172 beams increases with the incident electron energy, they
 173 correspond to tilted surface planes [28]. Croes et al. [25]
 174 has shown that the tilt angle of the *a*-domains can be
 175 estimated as $1.4^\circ \pm 0.1^\circ$. These *a*-domains can also be
 176 observed in bulk by cross-section TEM showing the pres-
 177 ence of 71° -type domain walls (figure 1(c)). Moreover the
 178 3D reciprocal space map measured by X-ray diffraction
 179 around the 222_c Bragg peak (*c* stands for pseudo-cubic
 180 coordinate) shows a splitting in four peaks. The major
 181 peak is at the lowest q_z momentum transfer value (35.41
 182 nm^{-1}) and can be assigned to the GeTe *c*-domains with
 183 a rhombohedral elongation of the unit cell in the $[111]$
 184 direction, *i.e.* perpendicular to the film (q_z is perpendic-
 185 ular to the surface). The three minor peaks are localized
 186 at higher q_z (36.73 nm^{-1}) and can be assigned to ferroe-
 187 lastic/ferroelectric *a*-nanodomains whose unit cells are
 188 stretched in the three remaining directions $[11\bar{1}]_c$, $[\bar{1}\bar{1}1]_c$
 189 and $[\bar{1}1\bar{1}]_c$ in pseudo-cubic coordinates. The *a*-domains
 190 have a polarization direction at 71° with respect to the
 191 surface normal, *i.e.* mainly in-plane. This corroborates
 192 the observation that GeTe films have a preferential out-
 193 of-plane ferroelectric self-poling state dominated by *c*-

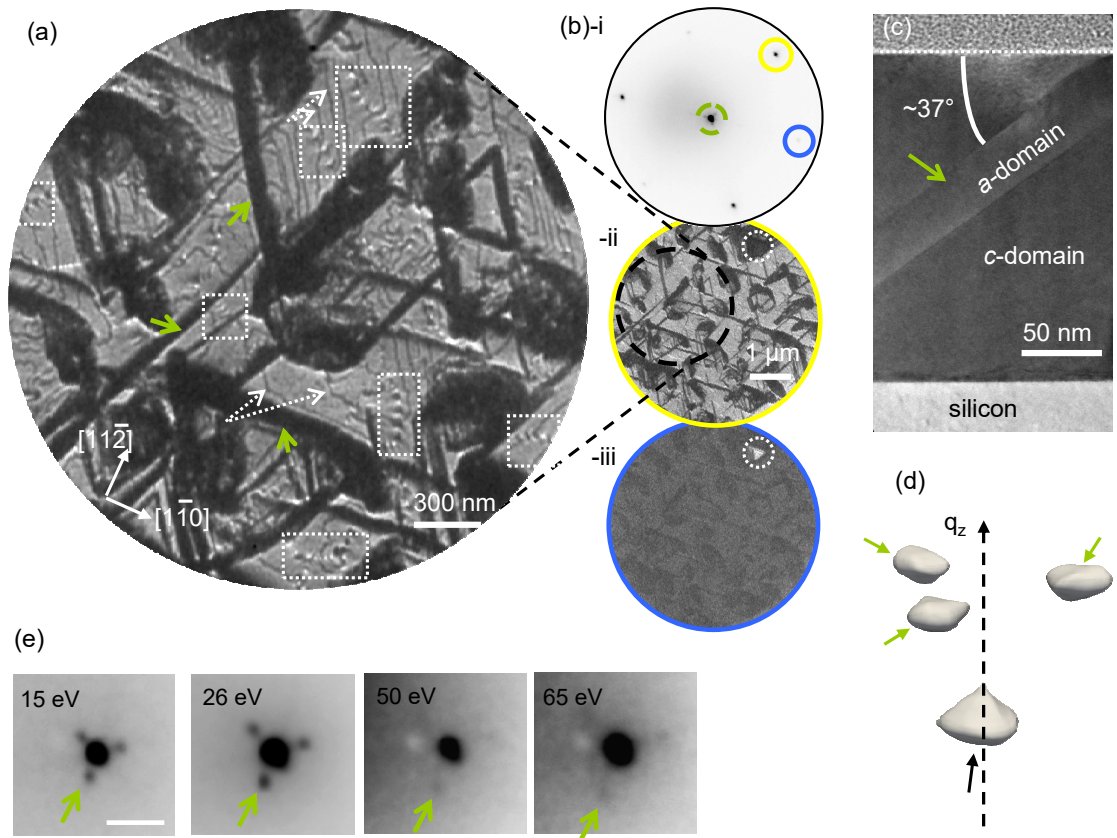


FIG. 1. (a) LEEM image of a 470 nm-thick GeTe thin film grown on Si(111)- $\sqrt{3} \times \sqrt{3}$ -Sb (Bright field mode, Electron energy: 26 eV). The contrast aperture selects only the reflected beam from the *c*-domains excluding the reflected beams from the *a*-nanodomains appearing as dark needles (green arrows). Row of defects from grain boundaries (see for instance in white dashed rectangles), ferroelectric *a*-nanodomains (green arrows), atomic steps (white dashed arrows). (b)-(i) LEED pattern of GeTe thin film (electron energy: 26 eV; incident beam diameter: $\varnothing=20 \mu\text{m}$). The threefold symmetry of the pattern arises from the (111) surface structure of GeTe. (ii) LEEM image in dark field mode (Electron energy: 26 eV) selecting the most intense diffracted beam (yellow circle in (i)). (iii) LEEM image in dark field mode (Electron energy: 26 eV) selecting the less intense diffracted beam (purple circle in (i)). Twinned grain (white dotted circles in (ii) and (iii)). (c) TEM cross-section of a 200 nm-thick GeTe thin film with medium resolution ($[110]$ zone axis). The green arrow show a *a*-nanodomain crossing the film. (d) iso-intensity representation (40000 counts) of a 3D reciprocal space map around $(00q_z)$ at $q_z \sim 36 \text{ nm}^{-1}$ (film thickness 800 nm). The green arrows show the diffraction peaks from the *a*-domains. (e) Close view around the (00) reflected beam of a LEED pattern (electron energy: 26 eV) at incident electron energy $E=15, 26, 50$ and 65 eV . The green arrows show the shift of the reflected beam by the *a*-domains with the incident electron energy.

194 domains [29].

195 In addition to domains and defects, LEEM measure-
 196 ments also show that the GeTe surface is made of atom-
 197 ically flat (111) terraces separated by atomic steps that
 198 are a few hundreds nanometers away. Since no island is
 199 visible on the terraces, this indicates that GeTe growth on
 200 Si(111) occurs *via* a steady state step-flow mode. There-
 201 fore during growth at 275°C the diffusion length of the
 202 species before nucleation of a 2D island is larger than
 203 the typical terrace width ($>100 \text{ nm}$). To better charac-
 204 terize the growth process, figure 2(a) shows a large scale
 205 STM image ($2 \times 2 \mu\text{m}^2$) of a 800-nm thick GeTe film.
 206 LEEM and STM show similar surface features (see sup-
 207 plementary material S1 [30]). The STM image derivative
 208 in figure 2(b) highlights the *a*-nanodomains elongated in

209 the $\langle 1\bar{1}0 \rangle$ direction since the surface plane is tilted. As
 210 for LEEM images, 3 domain orientations coexist. The
 211 surface also shows the presence of atomic steps corre-
 212 sponding to single Ge-Te bilayers (0.35 nm , inset in fig-
 213 ure 2(a)) as expected from the bulk lattice parameter
 214 of GeTe. This observation demonstrates that the GeTe
 215 growth proceeds *via* a direct incorporation of Ge and Te
 216 atoms at a bilayer step edge and not by successive growth
 217 of Ge and Te layers. This step-flow mode is associated
 218 with a well-defined orientation of atomic step edges with
 219 ascending steps in the $\langle 1\bar{1}2 \rangle$ direction (figures 2(a)-(b)).
 220 Considering a (111)-oriented surface there exists two low-
 221 energy step edges, the so-called A- and B-step edges
 222 (pseudo-fcc crystals), with in-plane orientations differing
 223 by 60° [31]. Since B-step (resp. A-step) edges are as-

224 cending (resp. descending) in the $\langle\bar{1}12\rangle$ direction (figure 279
 225 2(d)) thus the surface is dominated by B-step edges under
 226 growth conditions. From STM topography (see figure
 227 2(e)) corresponding to an intermediary stage of thin film
 228 growth (before the steady state step-flow process) both
 229 step edges can be observed on the surface. We can notice
 230 that A-step edges are straight whereas triangular notches
 231 are formed on B-step edges (see figure 2(e)). Since at late
 232 stage of the growth, all step edges are B-type we can infer
 233 that A-step edges grow faster than B-type (figure 2(c)).
 234 The sketch of the atomic structure of the GeTe surface
 235 (figure 2(d)) shows that the A-step edge is made with a
 236 $\{100\}$ microfacet whereas the B-step edge is made with
 237 a $\{111\}$ microfacet. Therefore a A-step edge is stoichio-
 238 metric in Ge-Te and is non-polar whereas a B-step edge is
 239 made of a single element and polar. Since B-step edges
 240 exhibit triangular notches, they spontaneously decom-
 241 pose into A-step edges and have a step edge termination
 242 without net charges. In addition the notches increase by
 243 a factor 2 the step edge length of B-steps with respect to a
 244 straight step edge, thus the growth rate of these notched
 245 B-step edge is reduced which favors their presence at the
 246 surface during growth.

247 STM images reveal also that atomic steps are undis-
 248 turbed by the ferroelectric a -domains (see figures 2(a)-
 249 (b) and (e)). This observation is fully consistent with
 250 the result that the growth of GeTe thin films occurs
 251 at a sufficiently high temperature for the ferroelectric
 252 a -domains to be absent [25]. The a -nanodomains nu-
 253 cleate and grow during cooling to room temperature after
 254 thin film growth and do not modify the overall step
 255 organization. However the ferroelectric a -domains still
 256 have an influence on the morphology of the GeTe sur-
 257 face as the height profile in the neighborhood of the a -
 258 domains is non-symmetric (figure 2(e)-(f)). The surface
 259 of the GeTe c -domains is lower on one side of the a -
 260 nanodomains (in the $[11\bar{2}]$ direction) whereas it is higher
 261 and flat on the opposite side. This morphology is related
 262 to the difference of (111) inter-reticular distance d_{111} be-
 263 tween the c -domains and the ferroelectric a -nanodomains
 264 as well as the penetration angle of the a -nanodomains
 265 inside the GeTe film. The inter-reticular distances d_{111}
 266 can be directly compared from the position of the 222_c
 267 Bragg peaks measured by X-ray diffraction (figure 1(d)).
 268 They provide a quantitative estimate of the compression
 269 of the (111) crystallographic planes (3.74%) inside the
 270 a -nanodomains with respect to the c -domains. Since the
 271 a -nanodomains penetrate with a definite angle inside the
 272 film (see TEM in figure 1(c) for the 71° -type domain
 273 wall), then the lowering effect measured on the GeTe sur-
 274 face of c -domains occurs on one side, *i.e.* above the fer-
 275 roelectric a -nanodomains, while it is absent on the other
 276 side. The domain wall angle (37°) and the film height H
 277 provide a typical distance W over which the deformation
 278 of the GeTe surface extends $W \sim \frac{H}{\tan(37^\circ)} \sim 1.3H$.

B. Surface polarity of a -nanodomains

280 The ferroelectric a -nanodomains allow relaxing the in-
 281 ternal stress induced by the substrate into the GeTe thin
 282 film [25]. In addition to the epitaxial stress at the in-
 283 terface, the free surface may also relax and this point is
 284 all the more crucial for polar surfaces [14]. However on
 285 the surface of the GeTe c -domains, that is polar, no sur-
 286 face reconstruction is detected by LEED or STM. This
 287 result corroborates previous STM observations of the sur-
 288 face of GeTe [33] and DFT calculations that a pristine
 289 (*i.e.* unreconstructed) Te-covered (111) surface is ener-
 290 getically favorable [32]. Considering the ferroelectric a -
 291 nanodomains, microdiffraction measurements (μ -LEED,
 292 beam diameter $\varnothing=300$ nm) on one single a -nanodomain
 293 give some information on the crystallographic structure
 294 (figure 3(a)). First the shift of the reflected beam can
 295 be assigned to the local tilt angle ($\sim 1.5^\circ \pm 0.2^\circ$) of the
 296 a -domain surface in the $[11\bar{2}]$ direction with respect to
 297 the GeTe c -domain [25]. This typical tilt angle is in ade-
 298 quation with the STM profile of the surface morphology
 299 (figure 2(f)) and corroborates macroscopic measurements
 300 of the shift of the reflected beam by LEED (figure 1(e)).
 301 Considering now the crystallographic lattice of the fer-
 302 roelectric domains, it appears that the diffracted spots
 303 of the a -nanodomain do not coincide with those of the
 304 c -domains, even after correcting for the rigid shift due
 305 to the tilt angle (figure 3(a)). To avoid systematic er-
 306 rors due to the distortion of the reciprocal space by the
 307 LEED setup we compare only the positions of the recipro-
 308 cal lattice points of the a -nanodomain and the c -domain
 309 that are localized in the same reciprocal space area. The
 310 reciprocal lattice of the a -nanodomain is slightly com-
 311 pressed by $2.2 \pm 0.2\%$ in the $[11\bar{2}]$ direction. We deduce
 312 that the in-plane lattice of the a -nanodomain is a dis-
 313 torted hexagon (figure 3(b)) with a monoclinic unit cell
 314 ($a'=b'=0.427$ nm, angle= 121.4°) whereas the c -domains
 315 have a hexagonal unit cell ($a=0.418$ nm, $b=0.418$ nm,
 316 angle= 120°). This result also perfectly matches the
 317 lattice of the GeTe a -nanodomains measured by X-ray
 318 diffraction when these latter are elongated along $[11\bar{1}]$
 319 and considering the (111) cut plane.

320 This result shows that the surface of the c -domains has
 321 a polarization axis aligned along the normal to the sur-
 322 face and a threefold symmetry whereas the surface plane
 323 of the a -nanodomains has a twofold symmetry axis. In
 324 addition the surface normal of the a -nanodomains is not
 325 parallel to the elongation axis of the rhombohedron but
 326 tilted by $\sim 71^\circ$. To address the surface relaxation mech-
 327 anisms of the polar a -nanodomains, we have performed
 328 high resolution STM images. Surface images of a 800
 329 nm-thick GeTe thin film show different features (figures
 330 4(a)-(b)). Flat areas are visible in the middle of the a -
 331 domain and regular rows are formed along the long side
 332 of the a -domain, *i.e.* parallel to the $[1\bar{1}0]$ direction. In
 333 addition very close to the a -domain edge, the row struc-
 334 ture changes to a two dimensional structure described as
 335 a scales structure. To determine the chemical termina-

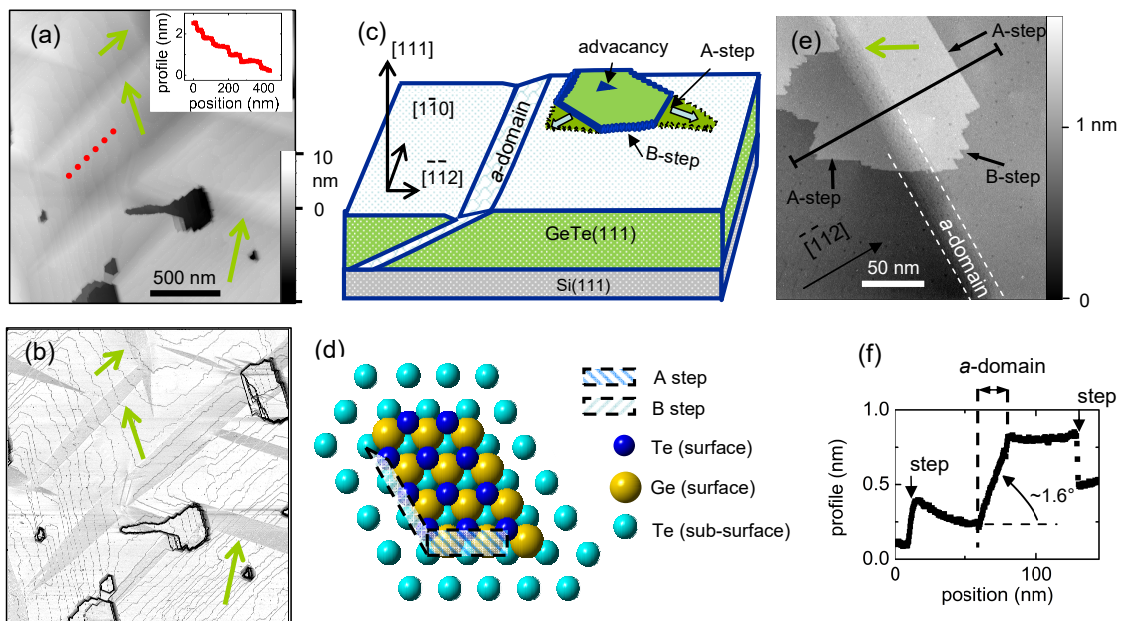


FIG. 2. (a) Large scale STM image of a 800 nm-thick GeTe thin film grown on Si(111)- $\sqrt{3} \times \sqrt{3}$ -Sb ($U = -1V$; $I = 20$ pA). Green arrows show ferroelectric a -nanodomains. Inset: profile on STM image (a) along dashed lines showing atomic steps at the surface (1 GeTe Bilayer (BL)=0.35 nm). (b) Image derivative of (a) to highlight ferroelectric a -nanodomains and atomic steps. (c) Scheme of the surface morphology of GeTe thin films on Si(111). (d) Scheme of A-step and B-step edge models. (e) Close view by STM of a 80 nm-thick GeTe thin film grown on Si(111)- $\sqrt{3} \times \sqrt{3}$ -Sb ($U = -1V$; $I = 20$ pA). Ferroelectric a -domains (green arrow and dotted guide lines), A-step and notched B-step edges (black arrows). (f) profile on STM image (e) (arrow: inclined profile due to the a -domain tilt).

336 tion at the surface of the a -nanodomains we can compare
 337 the surface profiles of a - and c -domains. The flat areas
 338 of a -nanodomains are ~ 150 pm below the surface of c -
 339 domains. This height corresponds approximately to the
 340 atomic spacing of the short Ge-Te bond [32]. Since c -
 341 domains are known to be Te-terminated, as deduced from
 342 XPS measurements [22] and surface energy minimization
 343 calculations [32], then the flat areas of a -nanodomains
 344 must be Ge-terminated. Concerning the row structure,
 345 it has a height modulation of 150 ± 20 pm and a peri-
 346 odicity of 5.1 ± 0.2 nm (figure 4(c)). This height modu-
 347 lation can be attributed to a missing row reconstruction
 348 of Te. Such a 1D surface modulation is consistent with
 349 the translation invariance of the c -domains along the long
 350 axis of the needle, *i.e.* in the $[1\bar{1}0]$ direction. This miss-
 351 ing row reconstruction is also observed in the context of
 352 metal surfaces with or without adsorption of adspecies
 353 (Pt(110) [34], Au(110) [35], O/Pd(110) [36]). The 2D
 354 scales structure observed initially close to the domain
 355 edge in figure 4(b) tends to cover the entire a -domain
 356 surface after long annealing at 200° C under UHV and
 357 forms a highly regular 2D network. The scales structure
 358 is made of missing Te rows in 2 directions. In addition
 359 triangular holes corresponding to GeTe bilayer vacancies
 360 can be found ($\sim 320 \pm 50$ pm). They preferentially occur
 361 in between Te scales or at the side of missing rows of Te
 362 (see figure 4(b)).

363 Based on our STM observations we have found that

364 kinetically, the surface termination of the ferroelectric a -
 365 nanodomains changes with a well defined process: (i) At
 366 first cooling, *i.e.* just after thin film growth, and for large
 367 a -domains (>100 nm width), the surface of a -domains
 368 show extended flat areas that are thus Ge-terminated.
 369 (ii) Upon annealing, the surface of the domains equi-
 370 librate by forming first a row structure (missing row
 371 reconstruction) and then (iii) a scales pattern that or-
 372 ders at long distance. The initial stability of the Ge-
 373 terminated flat areas in the middle of the a -domains may
 374 be counter-intuitive considering surface energies [32]. In
 375 figures 5-(a)-(b) is shown an atomically-resolved STM
 376 image of a Ge-terminated flat area in the middle of a a -
 377 nanodomain. From the Fourier Transform of the height
 378 of the flat area we can measure a hexagonal like pattern
 379 and a surface unit cell that is four times larger than the
 380 GeTe(111)-(1 \times 1) bulk terminated unit cell. Complemen-
 381 tary μ -LEED pattern at 6 eV incident energy shows that
 382 the surface is indeed 2×2 reconstructed and dark-field
 383 imaging with a 2×2 diffracted beam localizes the recon-
 384 struction on the a -nanodomains corroborating the STM
 385 analysis (figure 5-(c)). This type of surface reconstruction
 386 has been suggested on a similar IV-VI semiconductor
 387 system PbTe(111) by Rutherford Back Scattering mea-
 388 surements [37]. A 2×2 reconstruction has also been pro-
 389 posed to neutralize polar surfaces in the context of ionic
 390 materials or semiconductors and is known as the octopolar
 391 or alpha reconstructions [38–41]. The octopolar re-

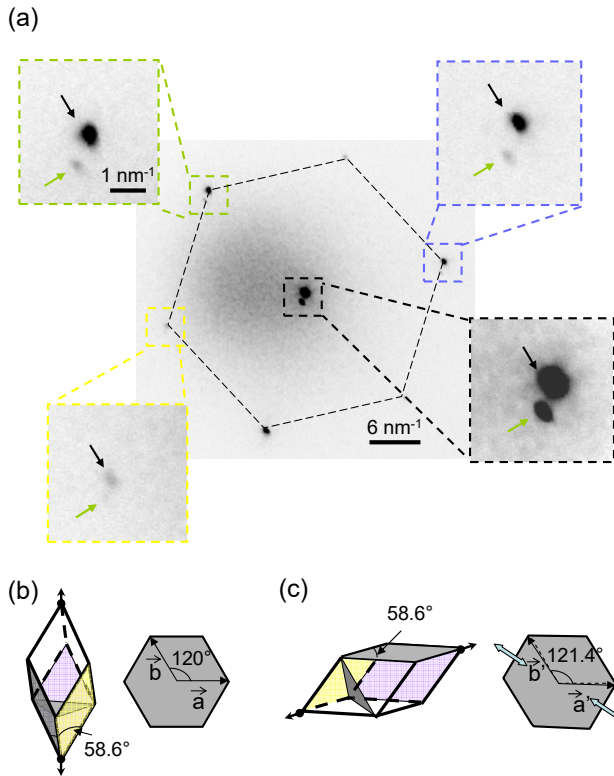


FIG. 3. (a) μ -LEED pattern of a GeTe thin film (800 nm-thick). The incident beam diameter is $\varnothing=300$ nm and the electron energy $E=26$ V. The incident beam illuminates one ferroelectric a -nanodomain and the surrounding GeTe layer. The hexagonal pattern of GeTe surface structure of the c -domain is detected (dashed hexagon). Insets: close views of reflected and diffracted spots. All spots are split into a major peak (black arrow) coming from the GeTe c -domain layer and a minor peak (green arrow) arising from the ferroelectric a -domain. The shift between the major and minor peaks is not a simple translation but changes with the selected diffracted spot). (b) Scheme of the crystallographic structure of GeTe c -domain and hexagonal surface lattice. (c) Same as (b) for a ferroelectric a -domain.

393 construction [42] is a pyramid-like structure obtained by
 394 keeping one quarter of atoms from the surface layer and
 395 three quarters of atoms from the subsurface layer. The
 396 alpha reconstruction derives from the octopolar one by
 397 removing the last atom of the surface layer (see geometri-
 398 cal model in figure 5-(d)). From the analysis of the STM
 399 images that indicates a Ge-terminated surface it is the al-
 400 pha reconstruction that is observed on the a -domains sur-
 401 face. In addition Deringer et al. has theoretically shown
 402 [32] that the alpha and octopolar reconstructions have
 403 similar surface energies on a polar (111)-GeTe surface
 404 (respectively 3.4-3.7 and 3.5 eV.nm⁻²). Despite the fact
 405 that the Te-terminated unreconstructed surface is the
 406 most stable (surface energy: 1.5-2.1 eV.nm⁻²) and is ob-
 407 served on the (111)-GeTe c -domains, it appears not to be
 408 the case on the a -nanodomains. We can notice that this

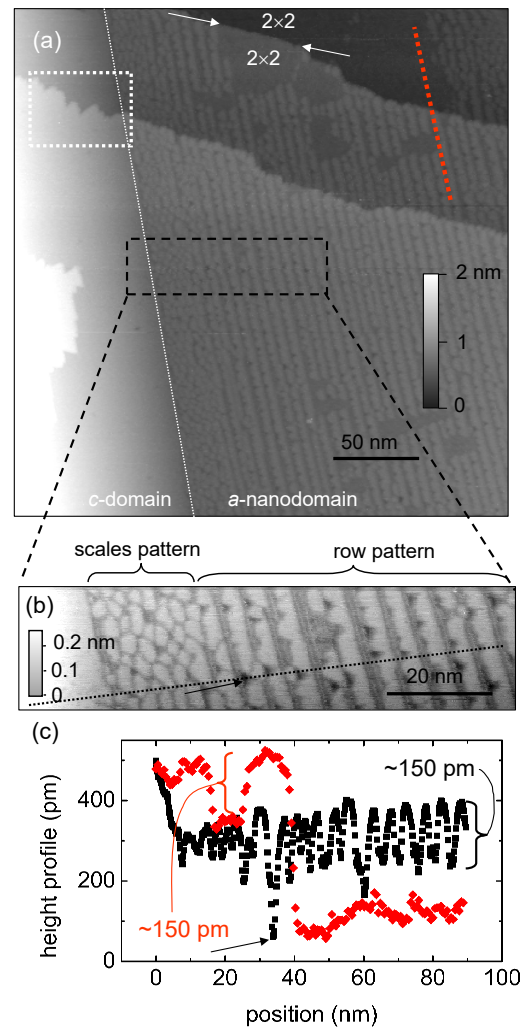


FIG. 4. (a) STM image ($U=-1$ V; $I=20$ pA) of the GeTe surface morphology (800 nm-thick film). A ferroelectric a -domain is on the right and the GeTe c -domain on the left. Flatness is imposed on the a -domain surface. Notched step-edge on the main GeTe layer (white dashed rectangle). Straight step-edge inside a 2×2 reconstructed area on the a -nanodomain (in between white arrows). (b) STM image ($U=-1$ V; $I=20$ pA) of the ferroelectric a -domain (from dashed rectangle on image (a)) with row and scale patterns. Black arrow shows a GeTe bilayer vacancy island. (c) STM height profiles along the 2×2 reconstruction (red dotted line in (a)) and row pattern (black dotted line in (b)). The black arrow shows the dip into the profile at the bilayer vacancy island in (b).

409 2×2 reconstruction induces a drastic change in the chem-
 410 ical termination of the surface (Ge) and stoichiometry
 411 (Ge₃Te₄) that may deeply modify the electronic proper-
 412 ties. In that respect we can also notice that B-step edges
 413 crossing flat 2×2 zones have no notch on the contrary to
 414 B-step edges on the GeTe c -domains (see figure 4-(a) at
 415 the top). This reinforces the proposal that the 2×2 sur-
 416 face reconstruction neutralizes the surface charges. The

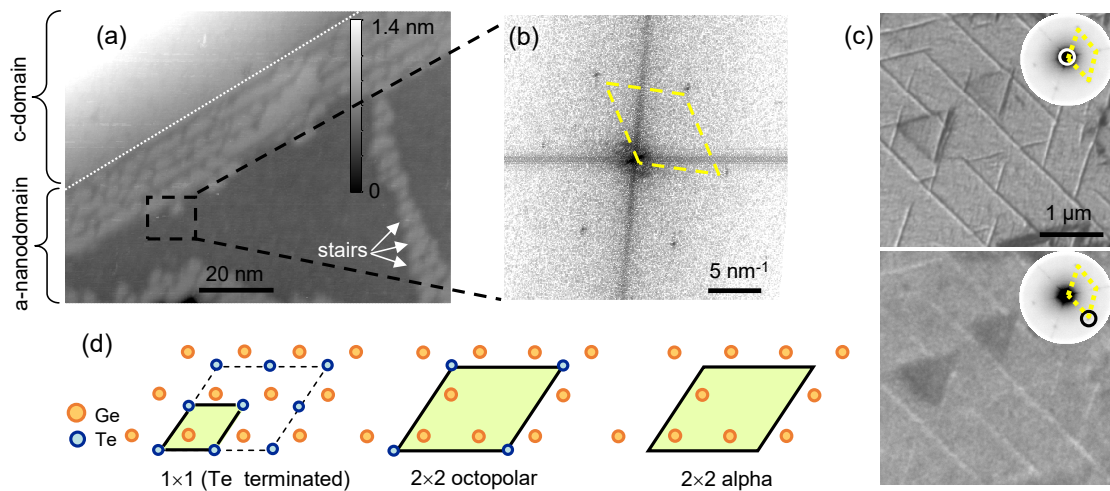


FIG. 5. (a) STM image of the surface of a a -nanodomain of a 1500 nm-thick GeTe thin film grown on Si(111)- $\sqrt{3} \times \sqrt{3}$ -Sb ($U = -1V$; $I = 20$ pA). (b) FFT of a high resolution STM image of the flat area of a a -nanodomain showing a 2D hexagonal lattice. (c) Bright-field (top) and dark-field (bottom) LEEM images at 6 eV of a 460 nm-thick GeTe thin film. The bright field mode is obtained selecting the reflected beams from both c - and a -domains (white circle in LEED pattern). The a -domains appear with a bright-dark contrast due to the hill-and-valley morphology (titled surface) and focusing conditions (see [45] and supplementary materials S7 and S8 in [25]). The dark field image is obtained selecting a 2×2 spot (dark circle in LEED pattern). Inset: μ -LEED patterns showing fine 2×2 spots from a 2×2 surface reconstruction. (d) Geometric model of the surface structure of a flat zone: 1×1 Te-terminated, 2×2 octopolar reconstruction; and 2×2 alpha reconstruction.

417 row pattern (Te-terminated) on the a -domains could be
 418 considered as a 12×1 surface reconstruction and may be
 419 compared to the 2×1 reconstruction (spinel reconstruction)
 420 as also theoretically predicted on polar (111)-GeTe
 421 surfaces [32] and detected by RHEED measurements on
 422 PbTe(111) thin films [43 and 44]. This reconstruction
 423 grows from the a -domain edges *via* stairs crossing the
 424 domain width (see figure 5-(a)). This growth mechanism
 425 shows that the advance of the reconstruction onto the
 426 surface is favored by the local environment of the atoms.
 427 At last the scales pattern is a stable reconstruction that
 428 stays onto the a -domains surface whatever further annealing
 429 or cooling processes. In figure 6-(a) is shown the
 430 surface of a GeTe a -nanodomain held at 220° C. The
 431 domain surface shows a regular pattern of scales which
 432 periodicity increases with temperature whereas the GeTe
 433 c -domains keep an unreconstructed surface with triangular
 434 *advacancy* islands coming from the GeTe congruent
 435 sublimation. The step edge retraction phenomena favors
 436 the fastest step edges in terms of kinetics of mass
 437 transfers, *i.e.* A-step edges that are straight and neutral.
 438 Atomically-resolved STM images of scales (figure
 439 6-(b)) show that this reconstruction has a very large unit
 440 cell ($\sim 4 \times 5$ nm²). We can deduce from the height pro-
 441 file that the surface is Te-terminated with missing rows
 442 in two directions. To understand the observed changes
 443 of reconstructions we infer that the 2×2 reconstruction
 444 and missing row pattern are metastable surface phases in-
 445 duced by a lack of Te. Indeed as Te is much more volatile
 446 than Ge [46 and 47] we can expect that adsorbed Te onto
 447 the surface is the minority species during GeTe growth.

448 Therefore the Te/Ge adatom ratio on the surface during
 449 deposition is slightly below 1. When growth is stopped
 450 and temperature decreased to room temperature, ferro-
 451 electric a -domains nucleate and grow. This process is
 452 due to the different linear expansion coefficients of GeTe
 453 and Si that induce a thermo-mechanical stress inside the
 454 film [25]. The occurrence of the a -nanodomains relaxes
 455 the global tensile stress by expanding the in-plane lattice
 456 parameter. Such a process only involves local rearrange-
 457 ments of atomic positions and the kinetics is expected to
 458 be much faster than mass transfers by diffusion. Conse-
 459 quently it does not provide enough time for the species
 460 to diffuse over large distances and optimize all surface
 461 structures. As the surface of the a -nanodomains and
 462 c -domains are in competition for Te, we observe that
 463 Te free *adatoms* cover primarily the c -domains. The
 464 a -nanodomains surface is therefore Ge-terminated and
 465 forms the 2×2 alpha reconstruction. After annealing the
 466 surface of a -nanodomains equilibrates *via* Te bulk diffu-
 467 sion and forms successively a missing row reconstruction
 468 and a scales structure that are more and more Te-rich.
 469 As the structures change from the domain edges we can
 470 infer that the Te atoms segregate from the domain walls.

471 III. CONCLUSION

472 In conclusion we have studied the growth and the struc-
 473 ture of the polar surface of ferroelectric GeTe thin films
 474 epitaxially grown on Si(111). The surface of the ferro-
 475 electric c -domains of GeTe has a rhombohedral elonga-

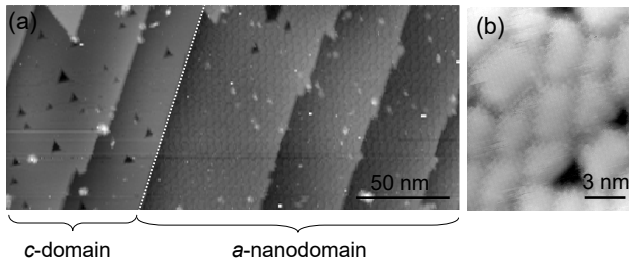


FIG. 6. (a) Large view STM image of the surface of a a -nanodomain of a 800 nm-thick GeTe thin film under annealing at 220°C (a -nanodomain on the right side of the dashed line). (b) High resolution STM image at RT of the scales structure onto a a -nanodomain surface. $U = -1\text{V}$; $I = 20\text{ pA}$.

tion perpendicular to the surface and is unreconstructed. Considering the ferroelectric a -nanodomains, the rhombohedral elongation is at 71° with respect to the surface normal. We have shown that the in-plane surface lattice is monoclinic and slightly tilted by 1.4° with respect to

the c -domains. The surface structure and polarity relax *via* a complex reorganization of surface atoms: a 2×2 alpha reconstruction, a missing row reconstruction and a 2D modulated structure form successively upon annealing. These surface relaxations release the surface energy involved in this low symmetry polar surface exhibiting a monoclinic unit cell and mainly a planar polarization. Our experimental measurements can be used as a playground to control ferroelectric domains and polarity in GeTe that will help to tune the surface Rashba effect *via* surface reconstructions.

Acknowledgements

The project leading to this publication has received funding from Excellence Initiative of Aix-Marseille University A*MIDEX, a french "Investissements d'Avenir" programme through the AMUtech Institute. This work has also been supported by the ANR grants HOLOLEEM (ANR-15-CE09-0012). We thanks Martiane Cabié (CP2M, Marseille, France) for lamella preparation of GeTe thin films by FIB, Lucio Martinelli (Synchrotron ESRF, Grenoble, France) for X-ray measurements and Salia Cherifi-Hertel (IPCMS, Strasbourg, France) for the fruitful discussions on ferroelectrics.

- 504 ¹ A. Gruverman, D. Wu, H-J Fan, I. Vrejoiu, M. Alexe, R. J. Harrison, and J. F. Scott, Vortex ferroelectric domains, *J. Phys.-Condens. Mat.* 20, 342201 (2008).
- 505
- 506 ² N. Balke, B. Winchester, W. Ren, Y. H. Chu, A. N. Morozovska, E. A. Eliseev, M. Huijben, R. K. Vasudevan, P. Maksymovych, J. Britson, S. Jesse, I. Kornev, R. Ramesh, L. Bellaiche, L. Q. Chen, and S. V. Kalinin, Enhanced electric conductivity at ferroelectric vortex cores in BiFeO₃, *Nat. Phys.* 8, 81 (2012).
- 507
- 508
- 509 ³ Y. L. Tang, Y. L. Zhu, X. L. Ma, A. Y. Borisevich, A. N. Morozovska, E. A. Eliseev, W. Y. Wang, Y. J. Wang, Y. B. Xu, Z. D. Zhang, and S. J. Pennycook, Observation of a periodic array of flux-closure quadrants in strained ferroelectric PbTiO₃ films, *Science* 348, 547 (2015).
- 510
- 511 ⁴ A. K. Yadav, C. T. Nelson, S. L. Hsu, Z. Hong, J. D. Clarkson, C. M. Schlepueetz, A. R. Damodaran, P. Shafer, E. Arenholz, L. R. Dedon, D. Chen, A. Vishwanath, A. M. Minor, L. Q. Chen, J. F. Scott, L. W. Martin, and R. Ramesh, Observation of polar vortices in oxide superlattices, *Nature* 530, 198 (2016).
- 512
- 513 ⁵ P. Shafer, P. Garcia-Fernandez, P. Aguado-Puente, A. R. Damodaran, A. K. Yadav, C. T. Nelson, S.-L. Hsu, J. C. Wojdel, J. Iniguez, L. W. Martin, E. Arenholz, J. Junquera, and R. Ramesh, Emergent chirality in the electric polarization texture of titanate superlattices, *P. Natl. Acad. Sci. USA* 115, 915 (2018).
- 514
- 515 ⁶ S. Das, Y. L. Tang, Z. Hong, M. A. P. Goncalves, M. R. McCarter, C. Klewe, K. X. Nguyen, F. Gomez-Ortiz, P. Shafer, E. Arenholz, V. A. Stoica, S. L. Hsu, B. Wang, C. Ophus, J. F. Liu, C. T. Nelson, S. Saremi, B. Prasad, A. B. Mei, D. G. Schlom, J. Iniguez, P. Garcia-Fernandez, D. A. Muller, L. Q. Chen, J. Junquera, L. W. Martin, and R. Ramesh, Observation of room-temperature polar skyrmions, *Nature* 568, 368 (2019).
- 516
- 517
- 518 ⁷ R. Ahluwalia, A. K. Tagantsev, P. Yudin, N. Setter, N. Ng, and D. J. Srolovitz, Influence of flexoelectric coupling on domain patterns in ferroelectrics, *Phys. Rev. B* 89, 174105 (2014).
- 519
- 520 ⁸ L. Jiang, Y. Zhou, Y. Zhang, Q. Yang, Y. Gu, and L.-Q. Chen, Polarization switching of the incommensurate phases induced by flexoelectric coupling in ferroelectric thin films, *Acta Mater.* 90, 344 (2015).
- 521
- 522 ⁹ H. Poettker and E. K. H. Salje, Flexoelectricity, incommensurate phases and the Lifshitz point, *J. Phys.-Condens. Mat.* 28, 075902 (2016).
- 523
- 524 ¹⁰ T.A. Aslanian and A.P. Levanyuk, Possibility of the incommensurate phase near Alpha-reversible-beta transition point in quartz, *Solid State Commun.* 31, 547 (1979).
- 525
- 526 ¹¹ E. Snoeck, A. Lubk, and C. Magén, Structural Characterization of Ferroelectric and Multiferroic Nanostructures by Advanced TEM Techniques, (John Wiley & Sons, New York, 2016), Chap. 10, pp. 275–324.
- 527
- 528 ¹² Z. L. Luo, H. Huang, H. Zhou, Z. H. Chen, Y. Yang, L. Wu, C. Zhu, H. Wang, M. Yang, S. Hu, H. Wen, X. Zhang, Z. Zhang, L. Chen, D. D. Fong, and C. Gao, Probing the domain structure of BiFeO₃ epitaxial films with three-dimensional reciprocal space mapping, *Appl. Phys. Lett.* 104, 182901 (2014).
- 529
- 530 ¹³ J. Chrosch and E.K.H. Salje, Temperature dependence of the domain wall width in LaAlO₃, *J. Appl. Phys.* 85, 722 (1999).
- 531
- 532 ¹⁴ C. Noguera, Polar oxide surfaces, *J. Phys.-Condens. Mat.* 12, R367 (2000).
- 533
- 534 ¹⁵ J. Goniakowski, F. Finocchi, and C. Noguera, Polarity of oxide surfaces and nanostructures, *Rep. Prog. Phys.* 71, 016501 (2008).
- 535
- 536 ¹⁶ B. Houchmandzadeh, J. Lajzerowicz, and E. Salje, Order parameter coupling and chirality of domain-walls, *J. Phys.-*
- 537

- Condens. Mat. 3, 5163 (1991).
- ¹⁷ B. Houchmandzadeh, J. Lajzerowicz, and E. Salje, Interfaces and ripple states in ferroelastic crystals - a simple model, *Phase Transit.* 38, 77 (1992).
- ¹⁸ V.K. Lazarov, S.A. Chambers, and M. Gajdardziska-Josifovska, Polar oxide interface stabilization by formation of metallic nanocrystals, *Phys. Rev. Lett.* 90, 216108 (2003).
- ¹⁹ S. Hong, S. M. Nakhmanson, and D. D. Fong, Screening mechanisms at polar oxide heterointerfaces, *Rep. Prog. Phys.* 79, 076501 (2016).
- ²⁰ D. Di Sante, P. Barone, R. Bertacco, and S. Picozzi, Electric Control of the Giant Rashba Effect in Bulk GeTe, *Adv. Mater.* 25, 509 (2013).
- ²¹ A. V. Kolobov, D. J. Kim, A. Giussani, P. Fons, J. Tomimaga, R. Calarco, and A. Gruverman, Ferroelectric switching in epitaxial GeTe films, *APL Mater.* 2, 066101 (2014).
- ²² C. Rinaldi, S. Varotto, M. Asa, J. Slawinska, J. Fujii, G. Vinai, S. Cecchi, D. Di Sante, R. Calarco, I. Vobornik, G. Panaccione, S. Picozzi, and R. Bertacco, Ferroelectric Control of the Spin Texture in GeTe, *Nano Lett.* 18, 2751 (2018).
- ²³ J. Krempasky, S. Muff, J. Minar, N. Pilet, M. Fanciulli, A. P. Weber, E. B. Guedes, M. Caputo, E. Mueller, V. V. Volobuev, M. Gmitra, C. A. F. Vaz, V Scagnoli, G. Springholz, and J. H. Dil, Operando Imaging of All-Electric Spin Texture Manipulation in Ferroelectric and Multiferroic Rashba Semiconductors, *Phys. Rev. X* 8, 021067 (2018).
- ²⁴ R. Wang, J. E. Boschker, E. Bruyer, D. Di Sante, S. Picozzi, K. Perumal, A. Giussani, H. Riechert, and R. Calarco, Toward Truly Single Crystalline GeTe Films: The Relevance of the Substrate Surface, *J. Phys. Chem. C* 118, 29724 (2014).
- ²⁵ B. Croes, F. Cheynis, Y. Zhang, C. Voulot, K. D. Dorkenoo, S. Cherifi-Hertel, C. Mocuta, M. Texier, T. Cornelius, O. Thomas, M.-I. Richard, P. Mueller, S. Curiotto, and F. Leroy, Ferroelectric nanodomains in epitaxial GeTe thin films, *Phys. Rev. Materials* 5, 124415 (2021).
- ²⁶ C. Mocuta, M.-I. Richard, J. Fouet, A. Stanescu, S. Barbier, C. Guichet, O. Thomas, S. Hustache, A. V. Zozulya, and D. Thiaudiere, Fast pole figure acquisition using area detectors at the DiffAbs beamline - Synchrotron SOLEIL, *J. Appl. Crystallog.* 46, 1842 (2013).
- ²⁷ Y. Liu, Y. Y. Li, S. Rajput, D. Gilks, L. Lari, P. L. Galindo, M. Weinert, V. K. Lazarov, and L. Li, Tuning Dirac states by strain in the topological insulator Bi₂Se₃, *Nat. Phys.* 10, 294 (2014).
- ²⁸ W.X. Tang, K.L. Man, H.C. Huang, C.H. Woo, and M.S. Altman, Growth shapes of Ag crystallites on the Si(111) surface, *J. Vac. Sci. Technol. B* 20, 2492 (2002).
- ²⁹ D. Kriegner, G. Springholz, C. Richter, N. Filet, E. Mueller, M. Capron, H. Berger, V. Holy, J. H. Dil and J. Krempasky, Ferroelectric Self-Poling in GeTe Films and Crystals, *Crystals* 9, 335 (2019).
- ³⁰ See Supplemental Material at [URL will be inserted by publisher] for a comparison of GeTe thin film surface morphologies by LEEM and STM.
- ³¹ M. Giesen, Step and island dynamics at solid/vacuum and solid/liquid interfaces, *Prog. Surf. Sci.* 68, 1 (2001).
- ³² V. L. Deringer, M. Lumeij, and R. Dronskowski, Ab Initio Modeling of alpha-GeTe(111) Surfaces, *J. Phys. Chem. C* 116, 15801 (2012).
- ³³ A. S. Frolov, J. Sanchez-Barriga, C. Callaert, J. Hadermann, V. A. Fedorov, D. Y. Usachov, A. N. Chaika, B. C. Walls, K. Zhussupbekov, V. I. Shvets, M. Muntwiler, M. Amati, L. Gregoratti, A. Y. Varykhalov, O. Rader, and V. L. Yashina, Atomic and Electronic Structure of a Multidomain GeTe Crystal, *ACS Nano* 14, 16576 (2020).
- ³⁴ E.C. Sowa, M.A. VanHove, and D.L. Adams, The missing-row model for the reconstructed Pt(110)-(1×2) Surface - A LEED intensity analysis showing multilayer distortions, *Surf. Sci.* 199, 174 (1988).
- ³⁵ I. K. Robinson, Direct determination of the Au(110) reconstructed surface by X-ray diffraction, *Phys. Rev. Lett.* 50, 1145 (1983).
- ³⁶ H. Tanaka, J. Yoshinobu, and M. Kawai, Oxygen-induced reconstruction of the Pd(110) surface - an STM study, *Surf. Sci.* 327, L505 (1995).
- ³⁷ K. Nakajima, K. Kimura, and M. Mannami, The (111) surface of PbTe observed by high-resolution RES, *Nucl. Instrum. Meth. B* 135, 350 (1998).
- ³⁸ F. Finocchi, A. Barbier, J. Jupille, and C. Noguera, Stability of rocksalt (111) polar surfaces: Beyond the octopole, *Phys. Rev. Lett.* 92, 136101 (2004).
- ³⁹ C. Franchini, V. Bayer, R. Podloucky, G. Parteder, S. Sunney, and F.P. Netzer, Density functional study of the polar MnO(111) surface, *Phys. Rev. B* 73, 155402 (2006).
- ⁴⁰ J. V. Lauritsen, S. Porsgaard, M. K. Rasmussen, M. C. R. Jensen, R. Bechstein, K. Meinander, B. S. Clausen, S. Helveg, R. Wahl, G. Kresse, and F. Besenbacher, Stabilization Principles for Polar Surfaces of ZnO, *ACS NANO* 5, 5987 (2011).
- ⁴¹ A Ohtake, J Nakamura, T Komura, T Hanada, T Yao, H Kuramochi, and M Ozeki, Surface structures of GaAs{111}A,B-(2×2), *Phys. Rev. B* 64, 045318 (2001).
- ⁴² D. Wolf, Reconstruction of NaCl surfaces from a dipolar solution to the Madelung problem, *Phys. Rev. Lett.* 68, 3315 (1992).
- ⁴³ Fuchs J., Z. Feit, and H. Preier, Reflection high-energy electron-diffraction intensity oscillations in IV-VI compound semiconductors, *Appl. Phys. Lett.* 53, 894 (1988).
- ⁴⁴ H. Wu, J. Si, Y. Yan, Q. Liao, and Y. Lu, Reconstructions and stabilities of PbTe(111) crystal surface from experiments and density-functional theory, *Appl. Surf. Sci.* 356, 742 (2015).
- ⁴⁵ K. M. Yu, A. Locatelli, and M. S. Altman, Comparing Fourier optics and contrast transfer function modeling of image formation in low energy electron microscopy, *Ultra-microscopy* 183, 109 (2017).
- ⁴⁶ M.V. Molchanov, A.S. Alikhanyan, V.P. Zlomanov, and L.V. Yashina, Mass spectrometric study of vapor composition over germanium telluride, *Inorg. Mater+* 38, 559 (2002).
- ⁴⁷ R. F. Brebrick, Partial Pressures and High-Temperature Thermodynamic Properties for the Germanium-Tellurium System, *J. Phase Equilib. Diff.* 40, 291 (2019).